

# Negative Ion Beam Production in an Ion Source with Chamfered Extraction Opening

M. TUREK\*

Institute of Physics, Maria Curie-Skłodowska University, Poland

The Particle-in-Cell method based numerical model of negative ion ( $H^-$ ) beam production in an ion source with chamfered extraction channel is presented. The model enables calculations of the charge density and electrostatic potential distribution as well as determination of extracted ion current. Influence of the chamfering angle on  $H^-$  density distributions and the obtained  $H^-$  current is under investigations. Major (by an order of magnitude) increase of the current is observed in the case of chamfered opening as the most of the extracted  $H^-$  ions are produced at the extraction channel walls. Changes of the extracted current due to  $H^-$  ion flux outgoing from the plasma grid are also studied. Current–voltage characteristics of the ion source both with non-chamfered and chamfered extraction channels are presented. Saturation of the C–V curve in the latter case for  $V_{ext}$  larger than 10 kV is observed. A transition of beam profile shape from a single maximum broad beam ( $V_{ext} < 0.5$  kV) through the ion beam with two maxima to a very intense broad ion beam ( $V_{ext} = 10$  kV) is presented and discussed.

DOI: [10.12693/APhysPolA.136.322](https://doi.org/10.12693/APhysPolA.136.322)

PACS/topics: 07.77.Ka, 07.05.Tp, 34.35.+a, 41.75.Ak, 41.75.Cn

## 1. Introduction

The neutral beam injection (NBI) systems making use of neutralisation of intense negative ion beams are crucial for plasma heating in prospective nuclear fusion devices like ITER [1, 2]. Negative ion ( $H^-/D^-$ ) beams of large current density (100–500 A/m<sup>2</sup>) are produced in the RF-inductively coupled ion sources with multi-aperture extraction grid systems [3, 4].

Numerical modelling of ion production, transport, and beam extraction is a powerful tool supporting design and optimisation of such devices. A multitude of advanced numerical models of negative ion beam extraction were developed [5–10] either focusing on a detailed description of the plasma near a single extraction opening surrounded by periodic boundary conditions or enabling a broader look at the cost of artificial increase of Debye length by scaling up the vacuum permittivity. The dispute concerning reliability of these approaches could be found in [11–13]. Nevertheless, different simulations provide the results showing e.g. that surface production of  $H^-$  due to conversion on the caesiated surface leads to potential well formation and  $H^-$  ion accumulation near that surface. Simulations including electron drift in the magnetic field proved also that the extracted  $H^-$  ion current grows with the magnetic filter strength [5, 14–16], which is consistent with the experimental results [17].

The paper presents the Particle-in-Cell 2D model of  $H^-$  ion transport and extraction in a single aperture system. The improved model not only more accurate calculations using a finer numerical mesh compared to that in our previous paper [18]. Moreover, it assumes that

negative ions can be created not only at caesiated (in order to lower its work function [19]) plasma grid parts facing the chamber but also at the chamfered surfaces of the extraction opening. The presented results were obtained using a self-consistent electrostatic code being a modified version of that described in [15, 16, 20, 21], taking into account also some particle-particle collisions.

Besides the concise model description, the paper presents the results of calculations of charge density and potential distributions as well as  $H^-$  extracted currents. The influence of the chamfered walls inclination angle on the  $H^-$  yield and charge distribution is discussed. Impact of the  $H^-$  flux outgoing from the chamber wall on the extracted current is also considered for different extraction channel geometries. The current-voltage curves obtained for different chamfering angles are compared. Evolution of the beam profiles with the change of extraction voltage due to the change of the place where the beam is emerging from is demonstrated and discussed in detail.

## 2. Numerical model

The model employed in the paper is based on the PIC (Particle-In-Cell) approach [22], assuming that each computational particle (also known as a pseudoparticle) represents a large group (thousands or millions) of particles behaving in exactly the same way. Such simplification reduces the size of a numerical task to a great extent. One needs, however, to take care of reasonable statistics in the plasma region i.e. each mesh cell should contain at least several tens of pseudoparticles. Moreover, the cell size should be smaller than the Debye length in the considered plasma.

Simulations were done using the two-dimensional model of an ionisation chamber of the length  $L = 4.5$  mm, width 5 mm and a single flat extraction electrode set on the negative extraction potential  $V_{ext}$  (see Fig. 1) and

\*e-mail: [mturek@kft.umcs.lublin.pl](mailto:mturek@kft.umcs.lublin.pl)

placed at distance  $d$  from the extraction opening. Negative ions and electrons are extracted through an extraction opening of conical symmetry. The inclination of the chamfered surfaces of the extraction opening is determined by the channel length  $h$  and its inner and outer radii  $r_i$  and  $r_o$ , respectively. The simulation area is covered by a rectangular  $150 \times 100$  grid. Cell sizes are set to  $\Delta x = \Delta y = 0.05$  mm. It is assumed that the chamber is initially filled with plasma of the charge density  $10^{16} \text{ m}^{-3}$  containing equal numbers of electrons and  $\text{H}^+$  ions. Each kind of real particles is represented by  $4 \times 10^6$  pseudoparticles uniformly distributed inside the chamber, with randomly directed velocities (at  $t = 0$ ), corresponding to the temperature  $kT = 1$  eV.

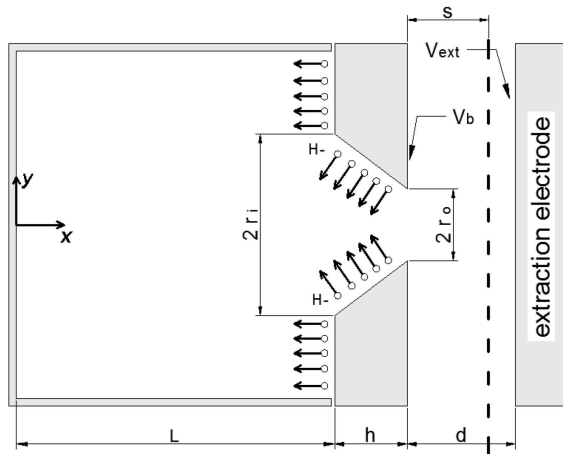


Fig. 1. Schematic drawing of the simulated system.

The potential distribution is found by solving the Poisson equation

$$\Delta V(x, y) = -\frac{\rho(x, y)}{\epsilon_0}$$

with the boundary conditions determined by electrodes. Charge density  $\rho(x, y)$  is found using the simplest nearest grid point approach as in [23], whereas Eq. (1) is solved using the successive over-relaxation method (SOR) as in our previous papers [15, 16, 24–28]. Once the potential distribution is found an electric field in the grid points is worked out by numerical derivation. This enables calculation of forces acting on the particles (also the nearest grid point scheme) and pushing particles forward according to the classical equations of motion. The equation of motions are integrated using the Verlet method [29]. After completion of this step new particle positions and velocities are found which enables calculation of new charge density distribution. The cycle is repeated as long as a desired state of simulation is achieved. The simulation timestep was set to  $0.2 \times 10^{-11}$  s in order to fulfil the Courant–Friedrichs–Lewy criterion [30]:

$$v \Delta t / \Delta x < 1, \quad (2)$$

as the typical particle velocities in plasma do not exceed  $v = 10^7$  m/s.

The code checks whether a particle hits electrodes where they are lost. In order to keep plasma density constant at the initial stage of simulation all lost  $\text{H}^+$  ions and electrons are replaced by new particles placed inside the chamber. After  $\sim 20000$  of steps some quasi-stationary potential and charge density distributions are achieved and  $\text{H}^-$  ions are injected into the chamber with the rate  $N_{\text{H}^-}$  per timestep. This magnitude simulates the rate of neutral-negative ion conversion that takes place at the caesium-covered surfaces in negative ion sources and is related to the Cs coverage. Negative ions are started not only from the inner surface of the front wall of the chamber (as in the previous paper [18]) but also from the chamfered surfaces of the extraction opening. It should be stressed that the flux of emitted  $\text{H}^-$  ions through the surface perpendicular to the  $x$  axis is the same for both emitting surfaces (inner wall and chamfered opening) in order to simulate incoming neutral-negative ion conversion taking place at these surfaces. The initial velocities of  $\text{H}^-$  ions correspond to  $kT = 0.25$  eV and their directions are random. The trajectories of significant part of negative ions are deflected towards the extraction electrode while positive ions are pushed inside the chamber. It should be mentioned that negative ion trajectories are randomly deflected by elastic collisions with other particles which is simulated using the Monte Carlo method based binary collision approximation [31]. The numbers of extracted electrons and ions are registered by the code and the particles are counted as they pass the distance  $s = 1.5$  mm from the extraction opening (see Fig. 1). Potential evolution in the chosen points inside the chamber and the total number of  $\text{H}^-$  ions inside the chamber is also registered. Charge density and electrostatic potential distributions are saved at the chosen moments of simulation.

### 3. Simulation results

Numerical simulations for  $r_o = 0.7$  mm and  $r_i$  varying in the range from 0.7 mm up to 2 mm were performed in order to check the influence of the  $\text{H}^-$  emission from the inclined surfaces near the extraction opening on the obtained currents and other working parameters of the ion source. Calculations were performed for  $V_{\text{ext}} = 2$  kV,  $d = 2.5$  mm, and 160000 time steps ( $0.32 \mu\text{s}$ ). Figure 2 shows the example of the potential evolution in the two points chosen along the ion source symmetry axis. Very fast potential oscillations are damped after  $\sim 30000$  timesteps. One should keep in mind that injection of  $\text{H}^-$  ions with the rate  $N_{\text{H}^-} = 300$  per timestep is started after 20000 steps. One can observe lowering of the potential inside the plasma chamber to approximately  $-10$  V as negative ions are introduced inside the chamber. It should be noticed that then the number of  $\text{H}^-$  ions contained in the chamber  $S_{\text{H}^-}$  grows slowly up to  $\sim 3 \times 10^6$  and the equilibrium is achieved. On the other hand, the extracted  $\text{H}^-$  ion current is stable after  $5 \times 10^4$  timesteps.

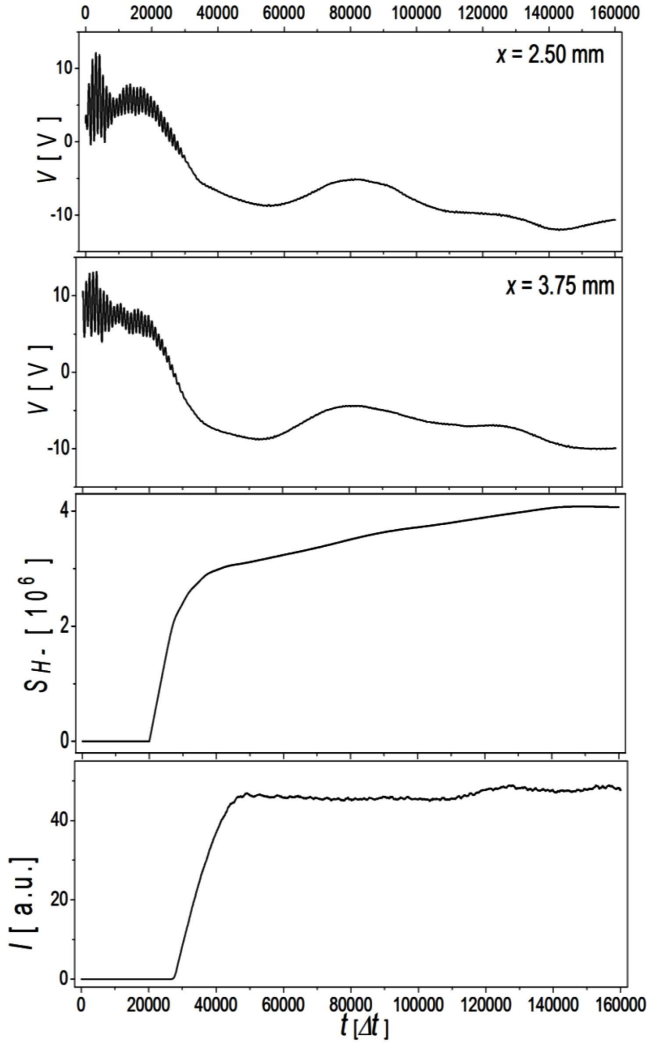


Fig. 2. Evolution of the electrostatic potential  $V$  in the two points inside the plasma chamber ( $x = 2.5$  mm,  $y = 0$ ) and ( $x = 3.75$  mm,  $y = 0$ ), the number of  $H^-$  ions inside the chamber  $S_{H^-}$  and the extracted  $H^-$  current.

It should be, however, explained that Fig. 2 presents the ion current averaged over 1000 timesteps in order to get rid of numerical noise.

Figure 3a presents changes of the extracted negative ioncurrent with  $r_i$ . The extraction channel surface inclination angle could be defined as:

$$\tan(\alpha) = \frac{r_i - r_o}{h}. \quad (3)$$

One can see that the current increases fast with  $r_i$  up to  $r_i = 1.7$  mm where the saturation is observed. The current for  $r_i = 1.7$  mm is  $\sim 8$  times larger than that in the case of unchamfered extraction channel  $r_i = r_o$ . Undoubtedly, this is due to the contribution from the ions produced at the inclined surfaces of the extraction channel. Figure 3b presents the ratio  $\delta$  of the numbers of extracted  $H^-$  ions produced at the back side of the grid and those created at the back side of the grid surfaces as the function of  $r_i$  (b).

those created at the extraction channel surfaces. This ratio decreases dramatically with  $r_i$  and for  $r_i = 1.7$  mm falls below 1%, which means that almost all  $H^-$  ions produced inside the chamber stay inside until they are neutralised. Figure 4 shows that increasing  $r_i$  and consequently  $\tan(\alpha)$  do not change the meniscus area. Larger ioncurrents are due to the increasing supply of  $H^-$  ions near the region of strong extraction field in the channel. Moreover, particles emitted from the inclined surfaces have velocity components toward the central part of the channel. It should be noticed that the arc-like structures directing toward the extraction electrode are formed as the largest part of extracted  $H^-$  ions comes from the regions near the extraction channel. This beam halo was already observed in the previous paper [32]. Lowering of the electrostatic potential near the  $H^-$  emitting inclined surfaces is observed in Fig. 4. This leads to the additional electric field component making the negative ions move along the channel walls towards the extraction electrode.

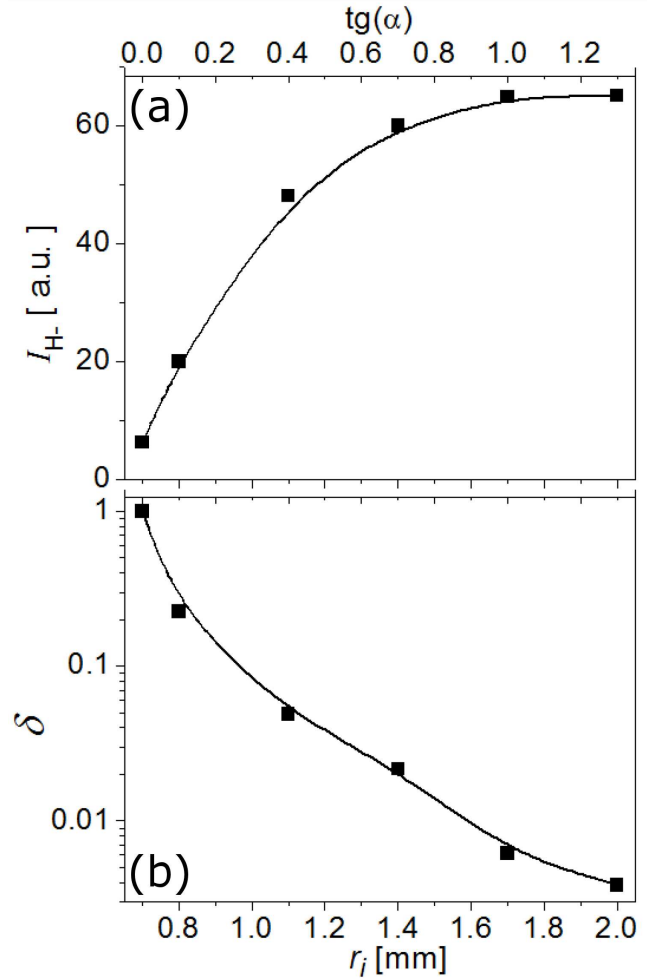


Fig. 3. The extracted  $H^-$  current (a) and the ratio  $\delta$  of numbers of extracted  $H^-$  ions produced at the back side of the grid and those created at the back side of the grid surfaces as the function of  $r_i$  (b).

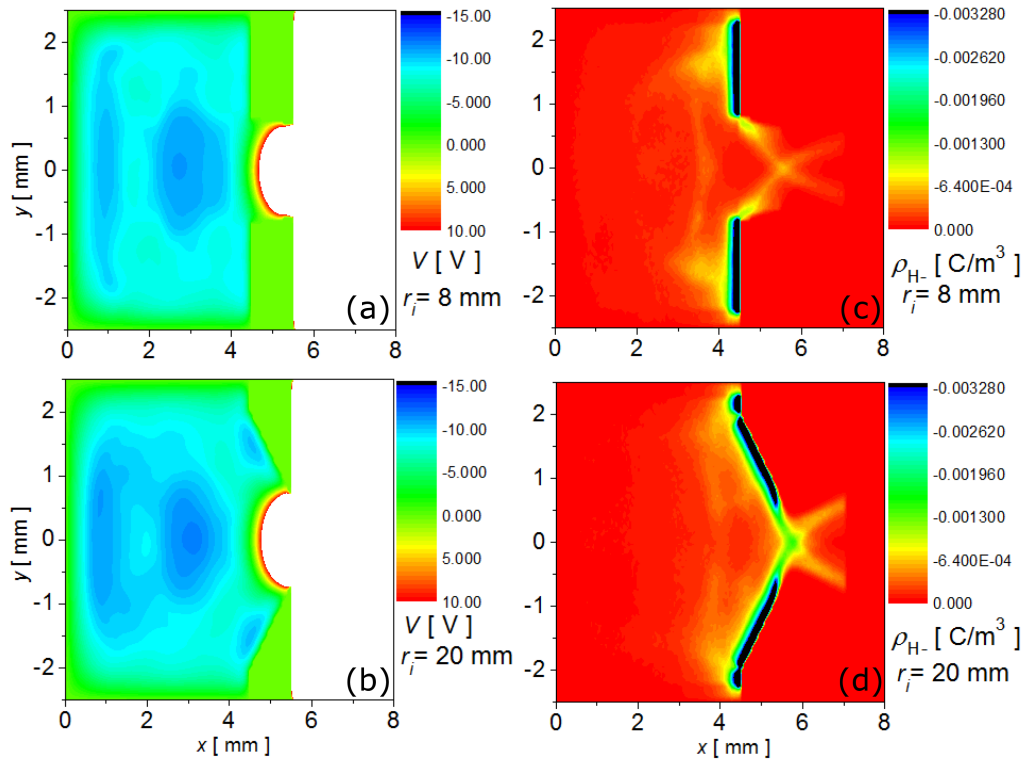


Fig. 4. Potential (a, b) and  $H^-$  charge density distributions (c, d) for the two different extraction opening geometries ( $r_i = 0.8$  mm and  $r_i = 2$  mm).

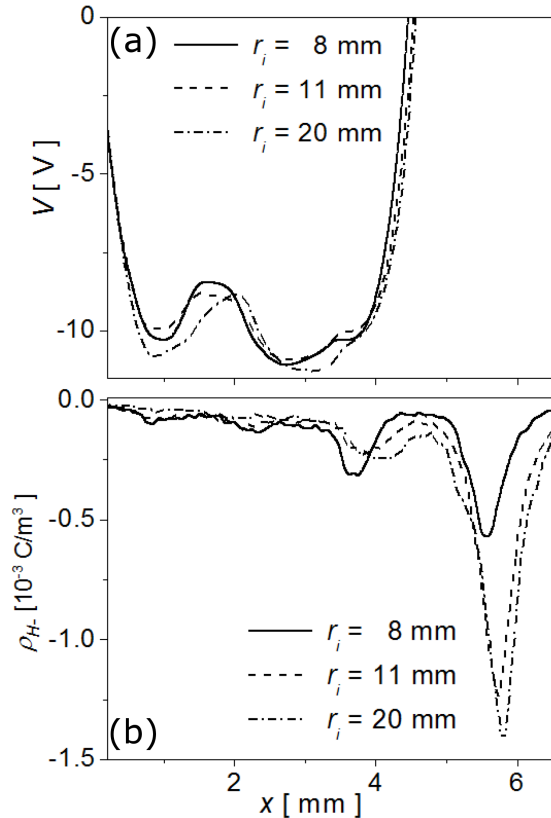


Fig. 5. Potential (a) and  $H^-$  charge density (b) profiles along the  $x = 0$  axis for different values of  $r_i$ .

The  $H^-$  charge density distribution deep inside the chamber also changes with  $r_i$  which can be better seen looking at the profiles presented in Fig. 5. The density inside the chamber gets smaller as  $\alpha$  increases due to the fact that more  $H^-$  ions are extracted very soon after their creation while in the case of  $r_i$  close to  $r_o$  most of them are directed into the chamber. On the other hand, the charge density in the beam area increases to more than twice its value.

The changes of the extracted  $H^-$  current due to the  $H^-$  flux outgoing from the plasma electrode wall ( $N_{H^-}$  parameter changing up to 700 ions per timestep) were also investigated. Calculations were done for two configurations of the extraction opening i.e. for  $r_i = r_o = 1.4$  mm and  $r_i = 0.7$ . One can easily see (Fig. 6) that the extracted currents are  $\sim 10$  times larger in the second case. Moreover, the curve obtained for  $t$   $r_i = r_o$  bends down with the increasing  $N_{H^-}$  although there is no saturation in the considered case.

Current-voltage characteristics of the ion source for  $N_{H^-} = 300$  and the two defined above extraction opening geometries were also evaluated. Simulations were done for  $V_{\text{ext}}$  up to 20 kV. Dependences of the extracted ion current are presented in Fig. 7. The yield in the case of chamfered extraction opening is  $\sim 10$  times larger than for  $r_i = r_o$  in the range of low extraction voltages ( $< 2$  kV). However, for  $V_{\text{ext}}$  larger than 5 kV the increase of the extracted current is smaller and saturation of  $I_{H^-}$  is observed for even larger  $V_{\text{ext}}$ .

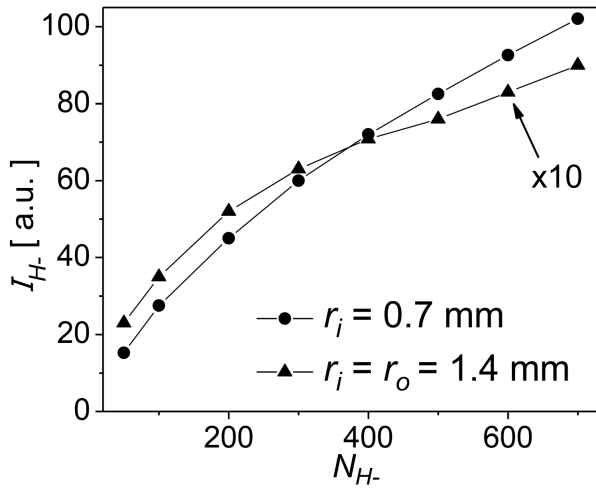


Fig. 6. Extracted  $H^-$  current as the function of  $N_{H^-}$  for the two different extraction channel geometries.

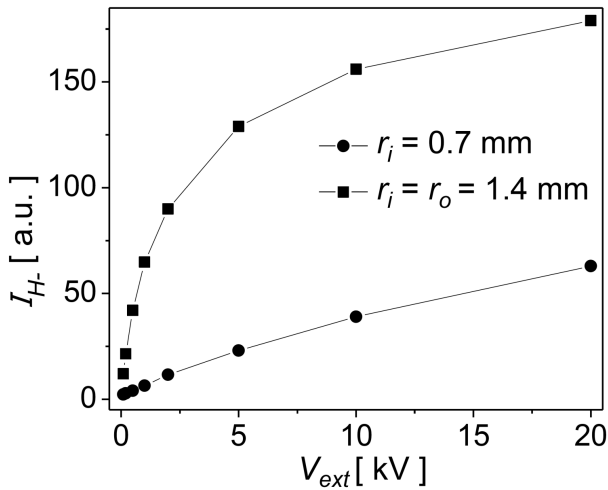


Fig. 7. Current–voltage curves for the two different extraction channel geometries.

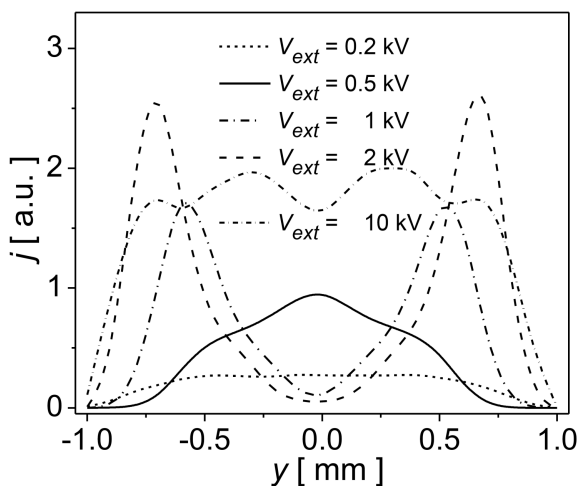


Fig. 8.  $H^-$  ion current density profiles at the distance  $s = 1.5$  from the extraction opening for different  $V_{ext}$ .

It should be mentioned that the beam profile varies in a very surprising way. Figure 8 presents the current density profiles registered at the plane placed 1.5 mm from the extraction opening. One can see transition from a very broad beam for low extraction voltages (200 V) through a typical single maximum beam profile for  $V_{ext} = 0.5$  kV to a two-maximum profile (a beam halo) as observed in the previous papers for the extraction voltages larger than 1 kV. The two maxima are initially more and more separated as  $V_{ext}$  grows but surprisingly for  $V_{ext} = 10$  kV the two maxima join together and a very broad intense ion beam with a small charge profile fluctuation is obtained. This behaviour is easier to understand when one looks closer at the final (after 160000 steps) negative ions charge density spatial distributions for different extraction voltages shown in Fig. 9.

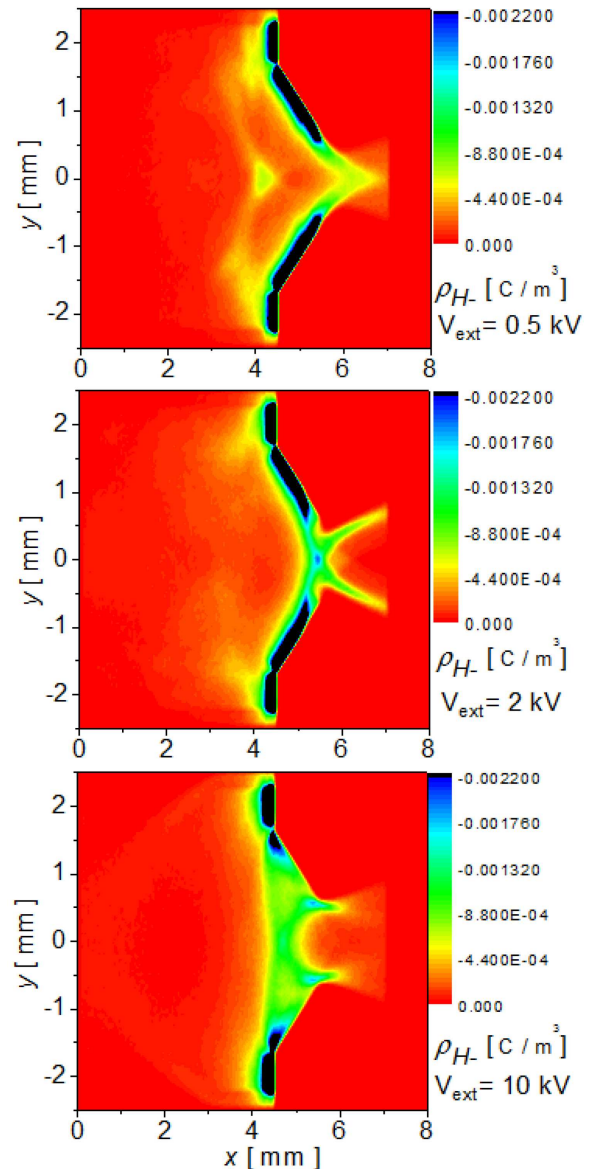


Fig. 9.  $H^-$  density distributions after 160000 timesteps for different  $V_{ext}$ .

For low extraction voltages (0.5 kV)  $H^-$  ions travel along the inclined surfaces of the extraction channels towards the extraction channel orifice. Two parts of the beam are emitted from the edges of the extraction channel and join just in front of the surface where the current density is registered. For higher  $V_{\text{ext}}$  the area of intense  $H^-$  emission moves along the extraction channel walls towards the chamber and the regions of depleted  $H^-$  concentration appear near the edges. The two beams emitted from the spots lying more deeply in the extraction chamber have a form of arcs crossing in the extraction orifice. As  $V_{\text{ext}}$  becomes higher the emitting spots move towards the chamber and the two beams are more and more distant. However, for even higher  $V_{\text{ext}}$  the beams pass the extraction orifice very near the channel edge. The outgoing beams are perpendicular to the electrode and are characterised by large spread. Consequently, they join in a single intense wide beam at relatively short distance (1.5 mm). Most of the  $H^-$  ions are attracted to the region of the wide extraction channel. This effect is even stronger for larger  $V_{\text{ext}} = 20$  kV as negative ions have a larger transverse velocity component due to the extraction field and no longer travel along the inclined walls.

#### 4. Conclusions

The Particle-in-Cell method based numerical model of negative ion surface production, transport, and beam extraction is presented in the paper. Evolution of potential, charge density distributions and extracted negative ion currents are investigated in a 2D model of an ion source with chamfered extraction opening. It was shown that the extracted negative ion current increases with the extraction channel wall inclination, making the ion beam production process by far more effective (an order of magnitude in the considered case). It was also demonstrated that in the case of the inclination angle  $\alpha = 45^\circ$  more than 99 percent of the extracted  $H^-$  ions are produced at the chamfered extraction channel walls. The advantage of the chamfered edge solution was confirmed also by dependences of extracted current on the  $H^-$  ion production rate  $N_{H^-}$ . The current voltage curves obtained in the case of non-chamfered and chamfered extraction channels were extracted-although the much higher currents are obtained using the chamfered extraction opening. The saturation of extracted current could be seen already for  $V_{\text{ext}}$  above 10 kV. As in the case of negative ion extraction of surface produced  $H^-$  ions through a non-chamfered extraction opening [32] a beam halo could be observed also in the case of chamfered opening. A complex evolution of the extracted beam current density profile (broad beam-beam with a halo effect intense broad beam) with the increasing  $V_{\text{ext}}$  was observed. This behaviour was a consequence of the fact that increasing the  $V_{\text{ext}}$  value changes the place the  $H^-$  ion beam comes from.

#### References

- [1] R. Hemsworth, A. Tanga, V. Antoni, *Rev. Sci. Instrum.* **79**, 02C109 (2008).
- [2] R. Hemsworth, H. Decamps, J. Graceffa, B. Schunke, M. Tanaka, M. Dremel, A. Tanga, H.P.L. De Esch, F. Geli, J. Milnes, T. Inoue, D. Marcuzzi, P. Sonato, P. Zaccaria, *Nucl. Fusion* **49**, 045006 (2009).
- [3] E. Speth, H.D. Falter, P. Franzen, U. Fantz, M. Bandyopadhyay, S. Christ, A. Encheva, M. Fröschle, D. Holtum, B. Heinemann, W. Kraus, A. Lorenz, Ch. Martens, P. McNeely, S. Obermayer, R. Riedl, R. Süss, A. Tanga, R. Wilhelm, D. Wunderlich, *Nucl. Fusion* **46**, S220 (2006).
- [4] W. Kraus, U. Fantz, P. Franzen, M. Fröschle, B. Heinemann, R. Riedl, D. Wunderlich, *Rev. Sci. Instrum.* **83**, 02B104 (2012).
- [5] S. Mochalsky, A. F. Lifschitz, T. Minea, *J. Appl. Phys.* **111**, 113303 (2012).
- [6] S. Mochalsky, D. Wuenderlich, U. Fantz, *Nucl. Fusion* **55**, 033011 (2015).
- [7] G. Fubiani, J.P. Boeuf, *Plasma Sources Sci. Technol.* **24**, 055001 (2015).
- [8] S. Nishioka, I. Goto, K. Miyamoto, A. Hatayama, A. Fukano, *J. Appl. Phys.* **119**, 023302 (2016).
- [9] G. Fubiani, L. Garrigues, G. Hagelaar, N. Kohen, J.P. Boeuf, *New J. Phys.* **19**, 015002 (2017).
- [10] F. Taccogna, P. Minelli, S. Longo, *Plasma Sources Sci. Technol.* **22**, 045019 (2013).
- [11] F. Taccogna, P. Minelli, *New J. Phys.* **19**, 015012 (2017).
- [12] J.P. Boeuf, G. Fubiani, L. Garrigues *Plasma Sources Sci. Technol.* **25**, 045010 (2016).
- [13] L. Garrigues, G. Fubiani, J.P. Boeuf *Nucl. Fusion* **57**, 014003 (2017).
- [14] T. Sakurabayashi, A. Hatayama, M. Bacal, *J. Appl. Phys.* **95**, 3937 (2004).
- [15] M. Turek, J. Sielanko, P. Franzen, E. Speth, *AIP Conf. Proc.* **812**, 153 (2006).
- [16] M. Turek, J. Sielanko, *Vacuum* **83**, 256 (2009).
- [17] M. Bacal, J. Bruneteau, P. Devynck, *Rev. Sci. Instrum.* **59**, 2152 (1988).
- [18] M. Turek, *Acta Phys. Pol. A* **132**, 254 (2017).
- [19] U. Fantz, P. Franzen, W. Kraus, M. Berger, S. Christ-Koch, M. Fröschle, R. Gutser, B. Heinemann, C. Martens, P. McNeely, R. Riedl, E. Speth, D. Wunderlich, *Plasma Phys. Control. Fusion* **49**, B563 (2007).
- [20] M. Turek, K. Pyszniak, A. Drożdźiel, J. Sielanko, A. Latuszyński, D. Maćzka, Y.A. Vaganov, Y.V. Yushkevich, *Instrum. Exp. Tech.* **52**, 90 (2009).
- [21] A. Pyszniak, A. Drożdźiel, M. Turek, A. Latuszyński, D. Maćzka, J. Sielanko, Y.A. Vaganov, Y. V. Yushkevich, *Instrum. Exp. Tech.* **50**, 552 (2007).
- [22] C.K. Birdsall, A.B. Langdon, *Plasma Physics Via Computer Simulation*, McGraw-Hill, New York, 1985.
- [23] M. Brzuszek, M. Turek, J. Sielanko, *Annales UMCS Informatica AI* **5**, 201 (2006).

- [24] M. Turek, A. Drozdziel, K. Pyszniak, S. Prucnal, J. Żuk, *Przeegląd Elektrotechniczny* **86**, 193 (2010).
- [25] M. Turek, K. Pyszniak, A. Drozdziel, J. Sielanko, *Vacuum* **82**, 1103 (2008).
- [26] M. Turek, K. Pyszniak, A. Drozdziel, *Vacuum* **83**, S260 (2009).
- [27] M. Turek, *Acta Phys. Pol. A* **123**, 847 (2013).
- [28] M. Turek, *Acta Phys. Pol. A* **132**, 259 (2017).
- [29] W.C. Swope, H.C. Andersen P.H. Berens, K.R. Wilson, *J. Chem. Phys.* **76**, 637 (1982).
- [30] R. Courant, K.O. Friedrichs, H. Levy, *Math. Ann.* **100**, 32 (1928).
- [31] S. Ma, R.D. Sydora, J.M. Dawson, *Comp. Phys. Commun.* **77**, 190 (1993).
- [32] M. Turek, *Przeegląd Elektrotechniczny* **92**, 162 (2016).